# An investigation of a low Strouhal number oscillatory jet submerged in a thin rectangular cavity

by

Nicholas J. Lawson[1] and Malcolm R. Davidson[2]

[1]Department of Aerospace, Power and Sensors
Royal Military College of Science, Cranfield University,
Shrivenham, Wiltshire. SN6 8LA, U.K.

[2]G.K Williams Cooperative Research Centre for Extractive Metallurgy
Department of Chemical Engineering, The University of Melbourne,
Parkville, Vic. 3052, Australia

**ABSTRACT**

Laser Doppler anemometry (LDA) and cinematic particle image velocimetry (PIV) measurements of a low Strouhal number oscillatory jet are compared to two-dimensional computational fluid dynamic (CFD) model predictions. The LDA and PIV measurements are recorded from a water model consisting of a jet generated from a submerged entry nozzle (SEN) immersed in a rectangular cavity. The cavity has a width to depth ratio (W/H) ranging from $0.1< W/H < 1.0$ and width to length ratio (W/L) ranging from $0.1 < W/L < 0.5$. In the CFD model, the flow emerging from the nozzle is represented as an internal mass source, and the flow past the region occupied by the nozzle (the crossflow region) is incorporated using a flow resistance. The CFD model is developed using the commercial fluid flow software CFX4. Analysis of the temporal LDA and PIV data has found the jet to have sustained oscillations about the broad face of the cavity with Strouhal numbers based on nozzle diameter ranging from 0.001-0.011. LDA analysis of the crossflow between the SEN and cavity walls allowed more detailed characteristics of the jet to be studied and compared with the CFD model predictions. Further analysis of the experimental data indicated that for self-sustaining oscillations to be present there must be a feedback loop through the crossflow region that links the recirculation cells bounding the jet. With this loop present, the Strouhal number of the jet was found to be independent of Reynolds number for a fixed geometry but highly dependent on the cavity width to length ratio. In addition, changing the area available for crossflow did not significantly affect Strouhal number. The crossflow amplitude was found to peak in the range $0.25 < W/L < 0.38$ for the water model and 0.38 for the numerical model. Jet oscillation was also stable for a particular cavity geometric range as shown in figure 1. Comparisons of experimental Strouhal number with values derived from the numerical model were found to match to within 10% in most cases. Qualitative comparisons with full field experimental data were found to give good agreement with all the main flow features present in the numerical model.

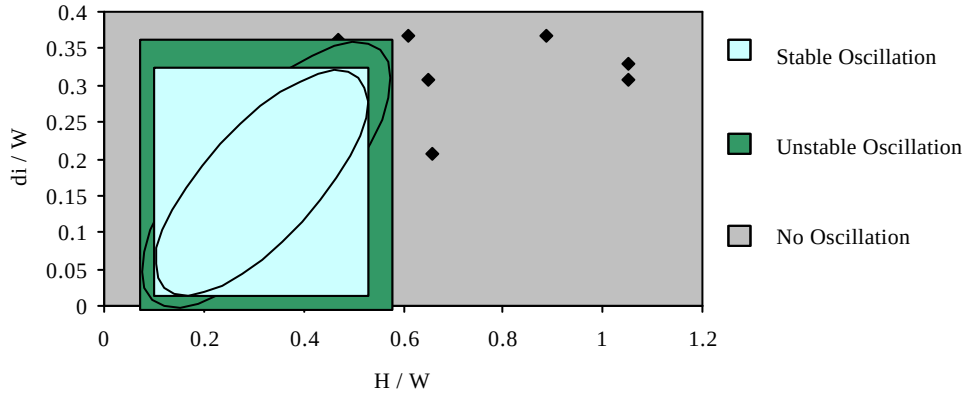


*Figure 1. Stability map for jet oscillation in cavity with fixed characteristic length of $L^* = 1050mm$*

## 1. INTRODUCTION

Low Strouhal number (St<<1) oscillatory jets can occur in thin rectangular cavities where the main jet or jets are bounded by typically one or two recirculation zones (Molloy, 1969, Rockwell, 1983, Shakouchi, 1989, Villermaux and Hopfinger, 1994, Nilles and Etienne, 1999). An example of such a flow can be found in thin slab continuous casting (e.g. of steel) which involves the injection of liquid metal using two lateral jets into a water cooled cavity through a Submerged Entry Nozzle (SEN) (Austin, 1992). As the metal solidifies the slab is drawn out of the bottom of the cavity and subsequently rolled into a sheet form. The cavity will generally have a width to thickness ratio of six or more to reduce rolling costs by providing a thinner cast slab output. Thin cavities, however, result in the formation of complex self-sustained oscillations by the jets with Strouhal numbers of St<<1; the oscillations are not related to any unsteadiness in the jet delivery system. This oscillatory behaviour entrains flux and impurities from the free surface which cause slab quality control issues. The impingement of the jets on the cavity walls can also cause problems with the shell thickness of the solidifying metal.

Low Strouhal number jet oscillatory mechanisms have not been as widely studied as the higher Strouhal number examples. In the latter case the oscillation mechanism has been shown to be related to the inherent instability of the shear layer giving Strouhal numbers of order St ≈ 1 (Rockwell, 1983). In the present case, however, the sustained oscillation occurs when the shear layer between the jet and the cavity is bounded by two recirculation zones. This generates jet oscillations with Strouhal numbers of St << 1. Previous studies of such low Strouhal number jet flows have attempted to isolate the mechanisms of oscillation by the use of techniques such as flow visualisation and pressure measurements (e.g Shakouchi, 1989, e.g. Villermaux and Hopfinger, 1994). Honeyands (1994), using a water model and flow visualisation, proposed that the oscillation is similar to that which occurs in a blind cavity (Molloy 1969) and is not related to any unsteadiness in the jet delivery system. Related flows that have been studied in more detail are confined jets in fluidic oscillators (e.g Shakouchi, 1989, Viets, 1975). In the present circumstance, the sustained oscillation relies on a feedback loop linking each side of the jet. The feedback loop allows movement of the recirculation zones up and down the cavity which in turn generates a crossflow in the nozzle region and an oscillation of the main jet. Without such a feedback loop, the recirculation zones will remain static and and this type of jet oscillation will not occur.

To date numerical predictions of low Strouhal number oscillatory flows have also been limited. Honeyands (1994) used a blind cavity arrangement with free out-flow conditions at the cavity top to model a sustained jet oscillation. More recently, Gebert et al (1998) predicted jet oscillation using a 2D model with outflow at the cavity bottom. In both cases, however, the lack of transient experimental data has limited further development of the numerical models. Therefore in what follows, numerical and experimental studies are presented which investigate such an oscillatory flow for a thin cavity. The experimental studies have initially concentrated on a single jet configuration for a range of cavity geometries and mass flow rates. Results from a 2D transient numerical model based on previous work by Gebert et al (1998) using the commercial code CFX are also presented and direct comparisons are made with the experimental data.

## 2. EXPERIMENTAL MODELLING

The experimental modelling consisted of three major parts including the water model rig, the laser Doppler anemometry (LDA) system and a cinematic particle image velocimetry (PIV) system. The following will now describe these parts in more detail.

### 2.1 Water Model Rig

To observe the oscillatory flow, a water model was constructed with maximum optical access for the LDA and PIV measurements. This was achieved by using a glass cavity with perspex inserts and where possible a glass SEN as shown in figure 2. The cavity had maximum dimensions of width W = 500mm, length L = 800mm and thickness H = 180mm although inserts were used to vary the width and thickness of the cavity to a minimum of W = 80mm and H = 55mm. The SEN had a range of internal dimensions of 18mm < $d_i$ < 38mm which could be varied by using a set of standard plumbing fittings and pipes. A 200 litre header tank mounted 500mm above the cavity top was used to supply flow to the SEN and isolate any unsteadiness from the main flow circuit. The flow rate into the SEN was controlled using a gate valve. The header tank was supplied from a reservoir below the cavity through a Harland 2kW centrifugal pump with the head maintained in the tank using a commercially available ballcock. To complete the flow circuit a manifold with a slot valve was placed between the cavity

bottom and the reservoir and was extended to produce an outflow below the reservoir waterline. This was found to prevent bubbles forming in the manifold outlet and then rising into the cavity.

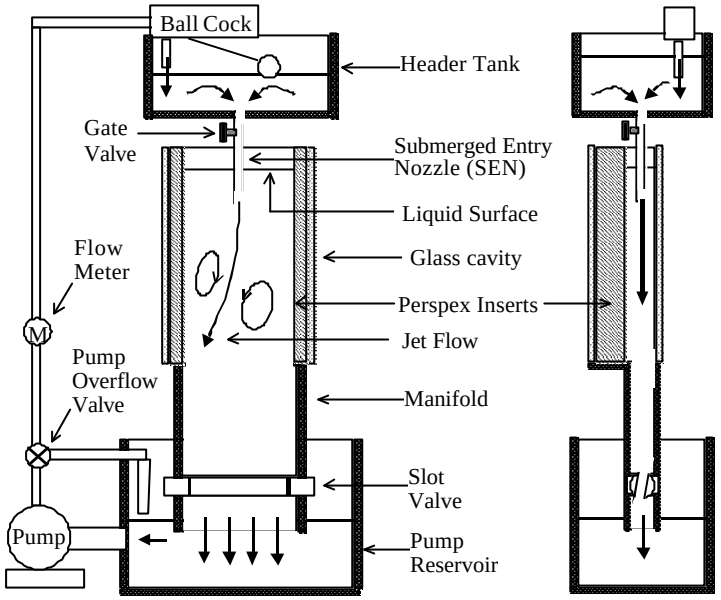


*Figure 2. Schematic of oscillatory jet water model*

One aspect of the water model that required careful consideration was the manifold design. Initial designs consisted of a row of outlet pipes with individual flow from gate valves. This was found, however, to bias the flow outlet onto a particular side of the cavity depending on the outlet pipe settings. Therefore an alternative arrangement was tried using a slot shaped manifold and a slot valve to regulate the flow. This design resulted in even outflow across the width of the cavity and a stable, sustained jet oscillation. More details of this design can be found in Lawson and Davidson (1999).

The geometry of the cavity for both the experimental and numerical modelling is shown in figure 3 with all the major variables that are to be considered. The x-y-z origin position (0, 0, 0), the two crossflow measurement points – Point A and B and the two PIV measurement regions – Region A and B are also shown in figures 3a and 3b. It should also be noted that the grey region in figure 3c is the crossflow region for the computational model.

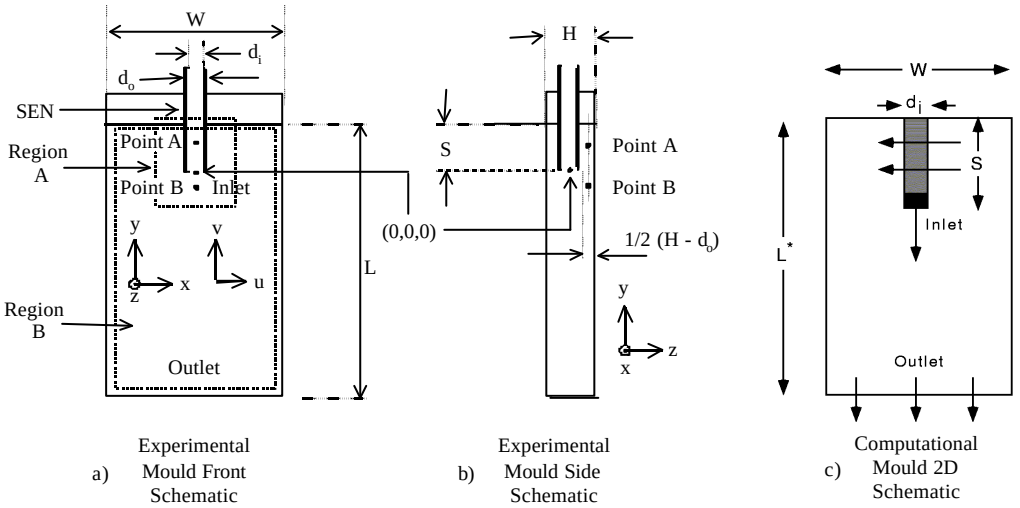


*Figure 3. Cavity Geometry (W = Cavity Width, L = Cavity Length, $L^*$= Dimensionless Length, H = Cavity Thickness, $d_o$ = SEN Outer Diameter, $d_i$ = SEN Inner Diameter, S = SEN Submergence)*

Experimental data was recorded for a number of cavity geometries, SEN geometries and mass flow rates by using flow visualisation, an in-house cinematic 2D PIV system and a commercial 2D LDA system. These systems will now be described in more detail.

## 2.2 LDA System

The LDA system was based on a Dantec two component FibreFlow system with a 58N40 FVA covariance processor. Figure 4 shows the overall measurement set-up. The two component LDA probe was mounted onto an x-y-z traverse with a 250mm focal length lens and used the green line (514.5nm) and blue line (488nm) from a 4W Coherent Argon Ion laser. A 40MHz frequency shift was used for directional discrimination with bandwidths varying from ±0.06MHz to ±0.6MHz to give corresponding velocity measurement ranges of ±0.2m/s and ±2.0m/s. The fluid was seeded with Fidene silver coated hollow glass spheres with a diameters of 10-30μm for acceptable flow fidelity. Seeding levels and laser power were adjusted during acquisition to ensure average data rates of 100Hz and sampling periods were set to 200-300s. These settings were based on *a-priori* knowledge of the flow where the jet oscillation frequencies where known typically between 0.03-0.1Hz.

The LDA data was processed into mean, rms and frequency data using standard residence time weighting algorithms and an FFT routine. These are described in detail by Lawson and Davidson (1999).

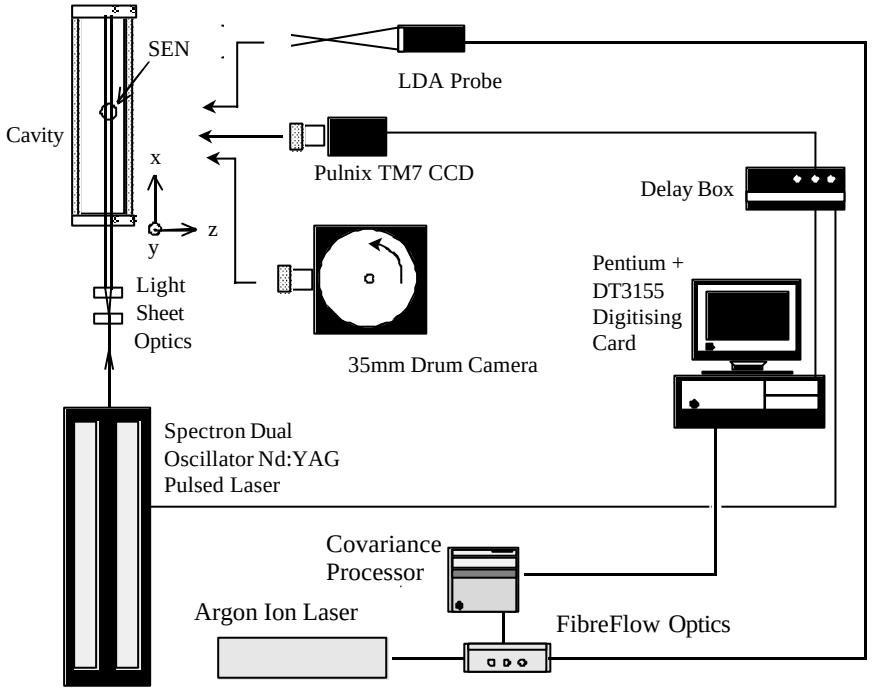


*Figure 4. Schematic of experimental measurement system*

## 2.3 PIV System

Two cinematic PIV systems were developed for the flow measurements. These included a high resolution photographic system and a lower resolution digital system to capture large and small imaging areas respectively from the cavity as shown in figure 4. The large and small areas correspond to Region A and B in figure 3. The light source used for both systems was a Spectron Laser Systems SL800 double pulsed Nd:YAG with 450mJ per pulse and pulse durations of 5ns. The maximum repetition rate of the laser was 12.5Hz.

The high resolution system was based on a 35mm drum camera and stored images on a 600mm diameter drum allowing a maximum of 50 full frame images per run (Lawson and Liow, 1998). In this case half frames were found to have sufficient resolution for region B and when digitised gave images with 1600 x 2400 pixels. During acquisition the camera shutter was simply opened and the laser double pulsed at the required repetition rate. This was typically set at 2Hz to capture the oscillatory features of the studied cycles. Use of such an arrangement also provided an automatic image shift between exposures thus removing any directional ambiguity during image processing (Adrian, 1986). The resultant images were then processed using autocorrelation techniques as

described previously with software written by the first author (Lawson et al, 1997). Typically 2000 vector points were output per image over an imaging area of 800mm x 500mm corresponding to a spatial resolution of 15.1mm.

The digital system was based on a Pulnix TM7AS CCD camera and a Data Translation DT3155 PCI board. Sequences of up to 80 frames with a resolution of 768 x 576 pixels could be stored at up to 12.5Hz depending on the flow to be studied. Synchronisation of the camera with the laser and board was achieved through the use of a delay box and video sync-stripper chip. This arrangement allowed the double pulse of the laser to be recorded onto the odd and even fields of the image as described by Lecordier et al (1994). Processing could then be completed using cross correlation methods. Typically 450 vector points were output per image over an imaging area of 200mm x 150mm corresponding to a spatial resolution of 8.3mm.

### 2.4 Flow Measurements

The experimental flow measurements were completed in three parts. These were the LDA measurements, the low resolution PIV measurements and the high resolution PIV measurements.

In the first case LDA data was primarily taken from the crossflow region, Points A and B in figure 3, and the jet centreline and outlet. Points A and B were chosen to study the temporal characteristics of the crossflow region after analysing more detailed data traverses in the same cavity area (Lawson and Davidson, 1999). Points A and B, positioned in a z position midpoint between the SEN and the cavity wall, ensured that when the SEN geometry was modified, the amplitude and frequency characteristics of the crossflow region could still be studied. Sets of data were taken for a range of SEN dimensions and cavity geometries as outlined previously (Lawson and Davidson, 1999).

For the PIV measurements the low resolution CCD system was used to study instantaneous flow structure in the crossflow region shown as region A in figure 3. This data was then directly compared to the 2D transient CFD results. Similarly, for the high resolution PIV system, full field measurements were taken from region B (figure 3) and the instantaneous flow structure compared to the CFD. In both cases data acquisition was limited to the base case with cavity dimensions of W = 500mm, H = 80mm, L = 1050mm, $d_I$ = 33mm, $d_o$ = 38mm.

## 3. NUMERICAL MODELLING

The commercial computational fluid flow solver CFX4 is used to implement the two-dimensional transient model of flow in the cavity. Only a brief overview of the model will be given here since a more detailed description, beyond the scope of this paper, can be found in Gebert et al. (1998) and Davidson et al. (1997). A two-dimensional rectangular model geometry is chosen because the cavity thickness is much less than the width. Figure 3c shows a schematic of the computational domain. To allow for crossflow past the region occupied by the SEN in a two-dimensional model, the inlet flow is represented as an internal mass source. In particular, the inlet is defined as the lower face of the black square in figure 3c which is removed from the computation domain. The top and side faces of this square are taken to be no-slip boundaries.

The grey region occupied by the SEN in figure 3c remains in the computational domain. In practice, resistance to crossflow through this region will occur by the blockage caused by the nozzle shaft. To account for this, a resisting force of the form $K|\mathbf{u}|\mathbf{u}$ is included, where $K$ is a constant. The value of dimensionless resistance coefficient $Kd_i/\rho$ =0.594 (based on $\rho$ = 1000 kg/m$^3$) is used here to give the "best" prediction for frequency in the base case (W = 500 mm and H = 80 mm).

The top boundary approximates the free surface as stationary and horizontal with a slip boundary condition. No-slip conditions together with standard wall functions are applied at solid walls., and zero normal gradients are specified at the flow outlet which comprises the entire bottom boundary. Turbulence is represented using the standard $\kappa$–$\varepsilon$ model.

## 4 RESULTS AND DISCUSSION

### 4.1 Crossflow Region

Figure 5 shows a sample of the LDA u component data from point A in the crossflow region for base case cavity conditions, i.e. W = 50mm, H = 80mm, L = 1050mm, $d_I$ = 33mm. The sinusoidal type nature of the flow oscillation is clearly evident as well as higher frequency fluctuations superimposed on top of the main oscillation. These higher frequency effects can be attributed to the turbulent nature of the flow where Reynolds numbers in the cavity range between $10^4 - 10^5$. Further examination of the frequency characteristics is shown in figure 6 which has been non-dimensionalised in terms of the cavity width W and jet diameter $d_i$.

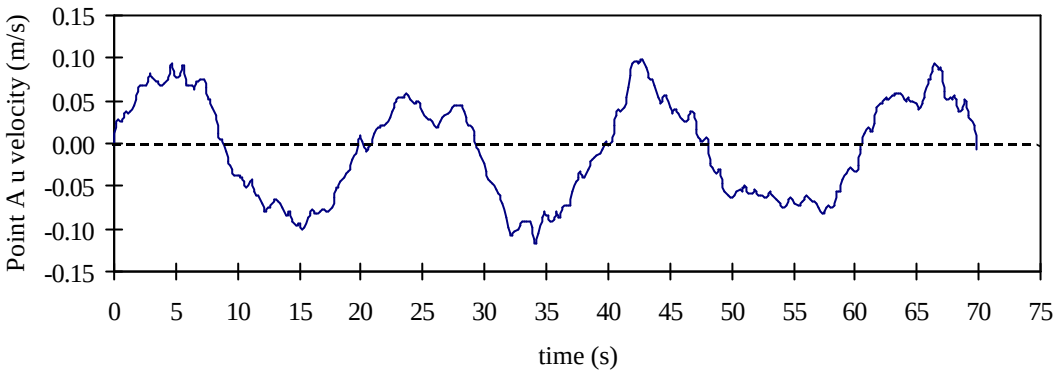


*Figure 5. LDA u component data for cavity based case (W = 50mm, H = 80mm, L = 1050mm, $d_I$ = 33mm)*

The results in figure 6a show the Strouhal number is independent of Reynolds number provided the cavity in plane geometric ratios or geometric similarly are maintained. This result is consistent with such high Reynolds number flows where viscous effects are limited to the cavity walls. Changes in geometry ratios in terms of width and length, however, have a significant effect on dimensionless frequency. This is shown in figure 6a and 6b although in figure 6b the Strouhal number is largely independent of cavity depth H. Generally, a reduction in W/L results in an increase in Strouhal number to a point where the jet will cease to oscillate. The numerical model results are also included in figure 6b and compare well with experimental results. In figure 6a, the changes in geometry are represented by a scaling factor scaled with respect to the base case cavity length $L^*$ = 1050mm.

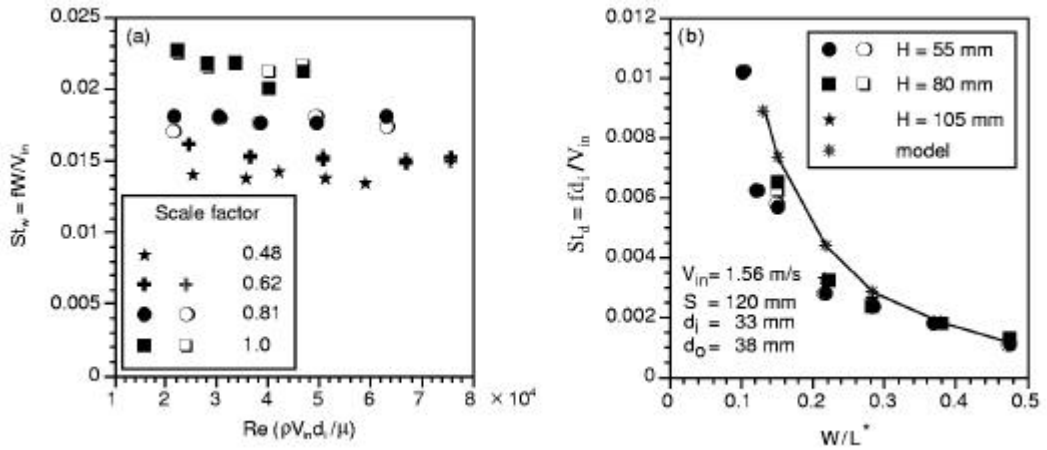


*Figure 6. Non-dimensional frequency characteristics for the cavity and jet*

The characteristics of crossflow peak amplitude at point A are shown in figure 7. Here increases in W/L initially cause an increase in oscillation amplitude to a peak followed by a reduction to a point where oscillation ceases. This characteristic can be explained by considering the limits of cavity geometry. In the case of an infinitely wide cavity, recirculation zones are unable to form thus preventing a feedback loop and so preventing jet oscillation. In the case of the cavity walls being equal to the SEN width, i.e. W = $d_o$, this will also prevent the formation of recirculation cells thus also stopping jet oscillation. Therefore in between these two limits, the recirculation zones will form and the oscillation amplitude will reach a maximum. Scaled numerical model results are also included in the graph and show good agreement up to the experimental maxima. After this point, however, the results diverge. Unfortunately, specific reasons for this divergence are currently unknown.

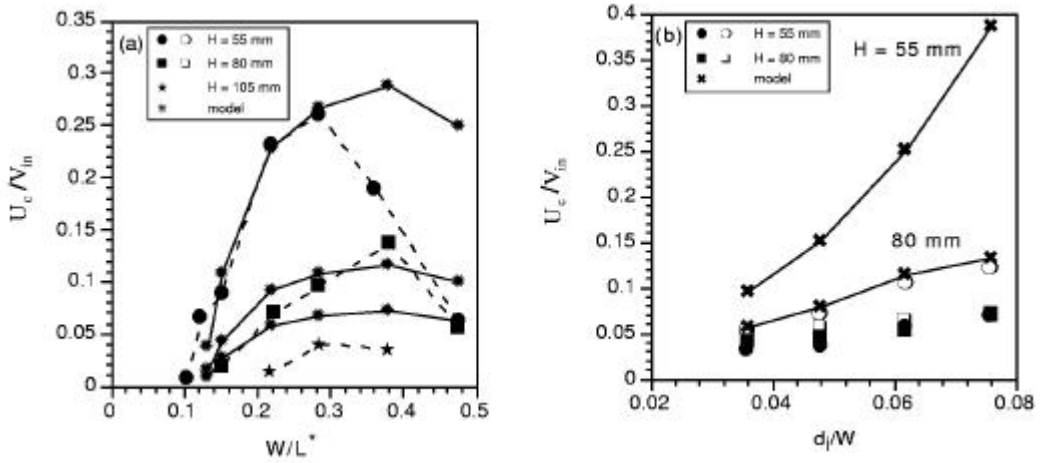


*Figure 7. Non-dimensional amplitude characteristics for the cavity and jet*

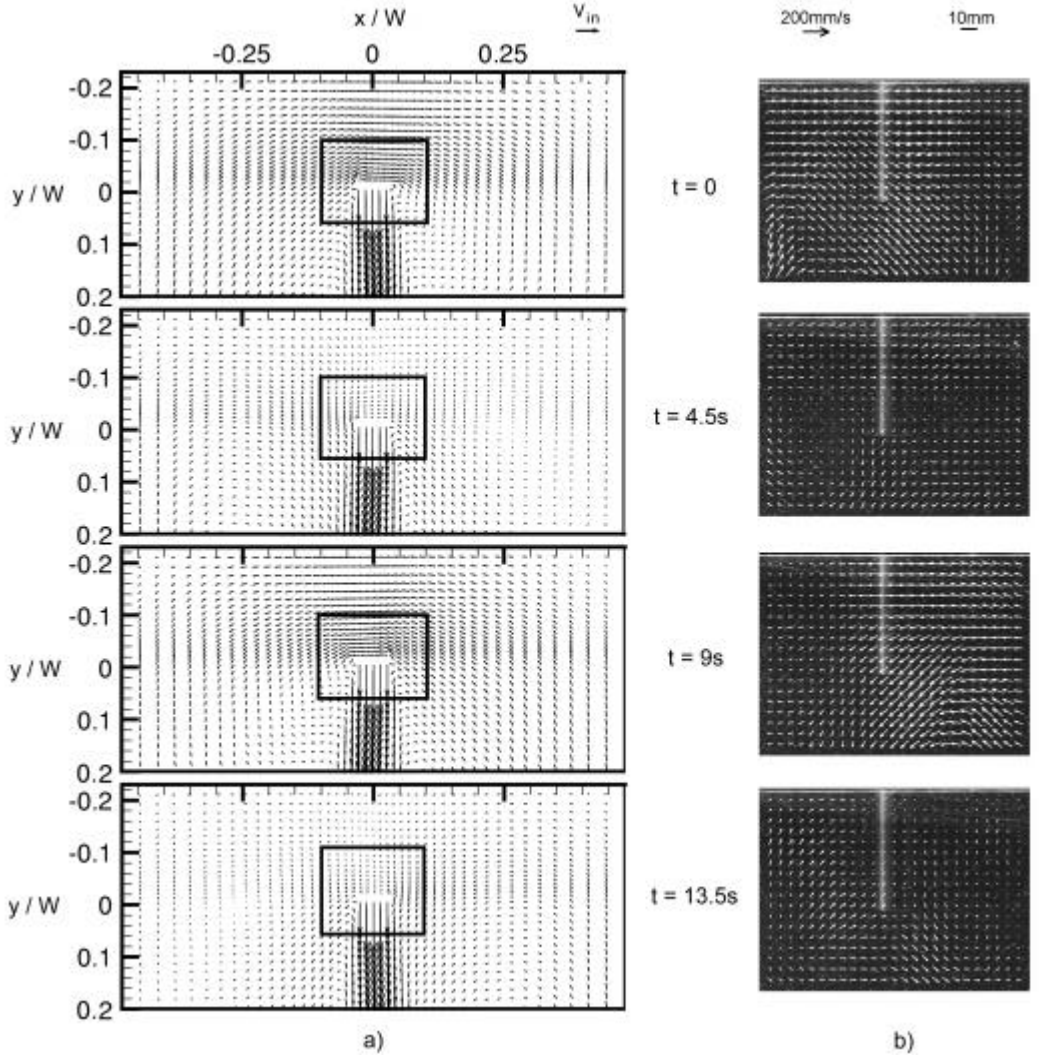


*Figure 8. Vector plots from the crossflow region a) predicted b) measured (region A)*

Figure 8 directly compares the low resolution PIV results taken from region A (figure 3) with the two-dimensional CFD crossflow predictions at equivalent instants of time in an oscillation cycle and for base case conditions. The box in the CFD results indicates the equivalent imaging area for the PIV data. The PIV results show the complexity of the crossflow region with large bulk movements of fluid occurring at various points in the cycle. This is in contrast to the CFD results where the bulk movements of fluid are more evenly distributed. The general pattern of the CFD flow field, however, matches well considering that the actual flow in the cavity is 3D in nature.

The large bulk movements of fluid in the real flow field are attributed to the turbulent nature of the flow, as before.

**4.2 Jet Region**

Figure 9a shows the mean centreline velocity profile in the jet for a range of SEN diameters. The transient CFD prediction is also included (solid line) as well as a CFD prediction for which the flow is constrained to be steady and symmetric (dashed line). The measured results show insensitivity to SEN diameter which would be expected for a high Reynolds number flow. It can also be seen that the oscillating jet decays faster than an equivalent theoretical steady jet. This is caused by the jet oscillation dispersing momentum laterally across a wider area thus reducing the flow velocity at the centreline.

Figure 9b shows the rms characteristics of the jet centreline for a range of SEN diameters, the transient and the steady CFD predictions as before. The turbulence of the measured flow is higher than the CFD prediction. This may be due to primary oscillation of the jet close to the nozzle which is not included in the numerical model.

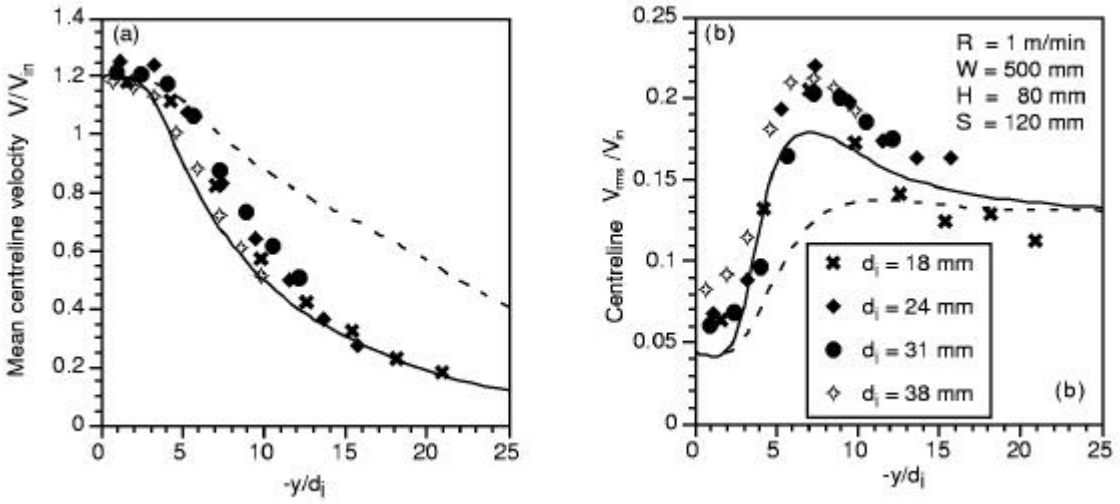


*Figure 9. Non-dimensional amplitude and rms characteristics from the jet core*

**4.3 Full Field**

Figure 10 shows the comparisons of the high resolution PIV results of the full flow field with CFD results at equivalent instants in time. The results are taken over one jet oscillation cycle at base case conditions. The measured results clearly show the two circulation zones bounding the main jet and the movement of the zones with the jet oscillation. Bulk fluid motion towards the crossflow region can also be seen at t = 0 and t = 9s although movement of this fluid around the SEN cannot be seen due to the centreline position of the measurement plane. Similar flow features can be seen in the CFD vector plots in addition to crossflow in the SEN region. In addition, further comparisons of the measured mean full flow field with the mean CFD flow field have shown excellent agreement to better than 20% of full scale velocity.

**4.4 Oscillatory Mechanism and Stability**

At this point it is convenient to discuss the oscillation mechanism. For such self-sustaining oscillations to be present there must be a feedback loop that links the recirculation cells bounding the jet. In the case of a single jet, feedback occurs through a crossflow area between the SEN and the cavity walls. Therefore removal of this feedback loop by reduction of the cavity width to the SEN diameter should prevent jet oscillation and this was shown to be the case by allowing $d_o = H$. For jet oscillation, however, particular geometric conditions must also be present to allow the recirculation zones and feedback loop to form.
This sensitivity of jet oscillatory behaviour with respect to cavity geometry can be summarised in figure 1. The plot shows the jet to have a stable oscillation for the range $0.1 < H/W < 0.5$ and $0.02 < d_i/W < 0.32$. This is limited, however, within a band where $d_i < W$ and $H/W < d_i/W + 0.4$. In the first instance $d_i < W$ is a physical limitation since the nozzle cannot have a width greater the cavity width. In the second instance it was found that if the

cavity was too wide with respect to the nozzle, i.e. a thin jet, the jet would not oscillate. This behaviour is possibly caused by out of plane movement of the jet and recirculation zones since the relatively wide cavity in this condition does not constrain these flow features thus preventing a stable feedback loop forming.

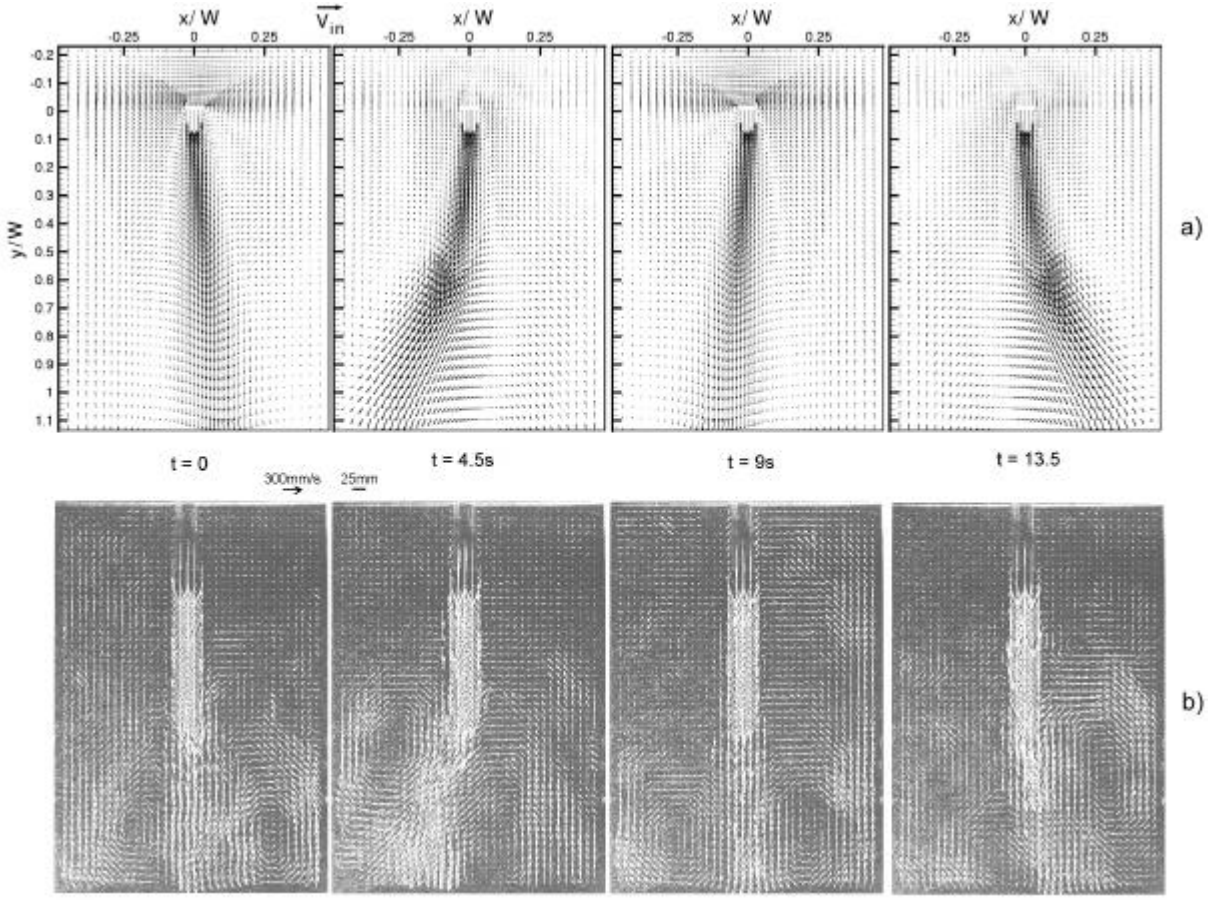


*Figure 10. Full field vector plots from a) predicted b) measured (region B)*

## 4. CONCLUSIONS

Pointwise and full field data have been measured from a low Strouhal number oscillatory jet submerged in a thin rectangular cavity and compared to a two-dimensional numerical model. The experimental data was recorded for a range of cavity and SEN geometries using a commercially available LDA system and an in-house cinematic low resolution and high resolution PIV system. Pointwise data was primarily taken the crossflow region which is the area between and adjacent to the SEN and cavity walls. The jet Strouhal number was found to be independent of Reynolds number for a fixed geometry but was highly dependent on the cavity width to length ratio (W/L) with a range of $0.011<St<0.001$ for $0.1<W/L<0.5$ respectively. Changing the area available for crossflow did not significantly affect the Strouhal number and the crossflow amplitude was found to peak in the range $0.25 < W/L < 0.38$ for the water model and 0.38 for the numerical model. Jet oscillation, however, was only stable for a particular geometric range. Comparisons of experimental Strouhal number with values derived from the numerical model were found to match to within 10% in most cases. Qualitative comparisons with full field experimental data were found to be good with all the main flow features present in the numerical model. Work is now ongoing to study the flow field generated by a bifurcated nozzle where initial results have shown the flow characteristics to be significantly more complex than for the single jet case.

## ACKNOWLEDGEMENTS

This work was supported by the Australian Research Council using facilities provided by the G.K. Williams Cooperative Research Centre for Extractive Metallurgy, a joint venture between the CSIRO Division of Minerals

and the Department of Chemical Engineering at the University of Melbourne. The authors would also like to thank Mr Tim Berrigan and the workshops of the Department of Chemical Engineering for their help and support during the project.

**REFERENCES**

Adrian R.J. (1986) Image shifting technique to resolve directional ambiguity in double-pulsed velocimetry. Applied Optics 25, 3855-3858.

Austin, P.R. (1992) Literature survey on modelling of continuous casting. BHP Research Unrestricted Report BHPR/PMR/R/92/044.

Davidson, M.R., Gebert, B.M., Rudman, M.J. & Lawson, N.J. (1997) Oscillating flow in a model of a thin slab casting mould. AEA Technology International Users Conference '97, Chicago, Illinois, October 6 - 19, 1997, pp.232 - 241.

Gebert, B.M., Davidson, M.R. & Rudman, M.J. (1998) Computed oscillations of a confined submerged liquid jet. Applied Mathematical Modelling 22, 843 – 850.

Lawson N.J., Coupland J.M., Halliwell N.A. (1997) A Generalised Optimisation Method for Double Pulsed Particle Image Velocimetry, Optics and Lasers in Engineering 27(6), p637-656.

Lawson N.J. & Liow J.-L. (1998) Low-cost design of 35mm drum camera for high-resolution, high-speed image analysis. Review of Scientific Instruments 69, 4195-4197.

Lawson N.J., Davidson M.R. (1999) Crossflow Characteristics of an Oscillating Jet in a Thin Slab Casting Mould, Journal of Fluids Engineering 121, 588-594.

Lecordier, B., Mouqallid, M., Vottier, S., Rouland, E., Allando D. & Trinte, M. (1994) CCD recording method for cross-correlation PIV development in unstationary high speed flow. Experiments in Fluids 1, 205-208.

Molloy, N.A. (1969) Oscillatory flow of a jet into a blind cavity. Nature 224, 1192 – 1194.

Nilles, P. & Etienne, A. (1991) Continuous casting today - status and prospects. Metallurgical Plant. and Technology International 6, 56-67.

Rockwell, D. (1983) Oscillations of impinging shear layers. AIAA Journal. 21, 645 - 664.

Shakouchi, T., Seumatsu, Y. & Ito, T. (1982) A study on oscillatory jet in a cavity. Bulletin of the JSME 25(206), 1258 - 1265.

Shakouchi, T., Seumatsu, Y. & Ito, T. (1982) A study on oscillatory jet in a cavity. Bulletin of the JSME 25(206), 1258 - 1265.

Viets H. (1975) Flip-flop jet design. AIAA Journal 13, 1375-1379.

Villermaux, E. & Hopfinger, E.J. (1994) Self-sustained oscillations of a confined jet: A case study for the non-linear delayed saturation model. Physica D 72, 230 - 243.